PCCP

ROYAL SOCIETY OF CHEMISTRY

PAPER

View Article Online
View Journal | View Issue

Cite this: *Phys. Chem. Chem. Phys.*, 2026, **28**, 5692

A hydrogen bond-driven strategy with ultrasound assistance for ultrafast and efficient recovery of PVDF nanoplastic from polymer solid electrolytes of all-solid lithium-ion batteries

Xuemin Jing,[a] Qianqian Liu,[a] Xingyu Shi,[a] Ziyi Sun,[a] Zhenghui Liu,[b] Zhenyang Li,[c] Na Ni[c] and Yu Chen *[a]

Received 29th December 2025,
Accepted 1st February 2026

DOI: 10.1039/d5cp05042a

rsc.li/pccp

Polyvinylidene fluoride (PVDF) based polymer solid electrolytes are crucial plastic components in all-solid-state lithium-ion batteries (ASLIBs). However, the large-scale application of PVDF-based solid electrolytes without proper treatment will cause persistent environmental contamination and resource waste, thus highlighting an urgent need for effective recovery strategies. Herein, we firstly propose a hydrogen bond-driven strategy with ultrasonic assistance for ultrafast and eco-friendly recovery of PVDF nanoplastic from polymer solid electrolytes of ASLIBs. Utilizing the proposed hydrogen bond-driven strategy, a maximum F leaching efficiency of 98.2% from PVDF nanoplastic can be attained within a short timeframe and under mild conditions using eco-friendly solvents. Compared with traditional methods, ultrasonic treatment exhibits a significantly improved leaching efficiency of approximately 88%. This ultrafast recovery and notable enhancement can be attributed to the breakdown of C–F bonds in PVDF, which is realized by regulating hydrogen bond networks in green solvents combined with ultrasonic treatment. This study presents a novel strategy for the green, rapid and significantly enhanced recovery of PVDF nanoplastic from spent polymer solid electrolytes of ASLIBs.

1. Introduction

All-solid-state lithium-ion batteries (ASLIBs) have emerged as promising candidates for next-generation energy storage systems, owing to their superior safety, high energy density, and long cycle stability compared to conventional liquid-electrolyte batteries.[1–3] As a key component of ASLIBs, polyvinylidene fluoride (PVDF)-based polymer solid electrolytes have garnered extensive attention due to their excellent chemical stability, mechanical robustness, and compatibility with electrode materials.[4–6] With the rapid expansion of the ASLIB market,[7] the large-scale production and subsequent retirement of PVDF-based solid electrolytes will cause plastic pollution and health risks that contradict with the sustainability goals of the energy storage industry.[8,9] The inefficient disposal of spent PVDF-based electrolytes not only leads to the loss of valuable F-containing resources but also poses potential ecological risks. Thus, developing effective, eco-friendly recovery technologies for PVDF-based solid electrolytes will be of great importance.[8,10,11]

In recent years, green solvents such as deep eutectic solvents (DESs),[12–16] ionic liquids,[17–26] supercritical fluids (SFs),[27,28] switchable solvents,[29,30] eutectic molecular liquids (EMLs),[31–34] low-melting mixture solvents (LoMMSs),[35,36] natural biomass soups (NBSs),[37,38] vegetable-/fruit-derived solvents (VFSs),[39] and superlong supercooling solvents (SSSs)[40,41] have gained attraction in sustainable separation and recovery processes, attributed to their low volatility, biodegradability, and tunable physicochemical properties.[35,42,43] Moreover, the regulation of hydrogen bond networks has emerged as a powerful tool to modulate intermolecular interactions in solution systems, enabling the selective dissociation of target components without disrupting their intrinsic structures.[44] Hydrogen bond-driven strategies have been successfully applied in fields such as polymer dissolution, pollutant removal, and resource recovery, demonstrating their potential to achieve efficient and mild separation.[45] Additionally, ultrasonic-assisted processes have been proven to accelerate mass transfer, enhance reaction kinetics, and promote bond cleavage through cavitation effects, offering a feasible approach to improve recovery efficiency.[46,47]

[a] *Department of Chemistry and Material Science, Langfang Normal University, Langfang 065000, Hebei, China. E-mail: yuchen@iccas.ac.cn; Fax: +86-316-2112462; Tel: +86-316-2188211*
[b] *School of Pharmaceutical and Chemical Engineering, Taizhou University, Taizhou 318000, Zhejiang, China*
[c] *Langfang Qingyue Environmental Technology Co., Ltd, No. 3 Huayuan Road, Economic and Technological Development Zone, Langfang 065000, Hebei, P. R. China*

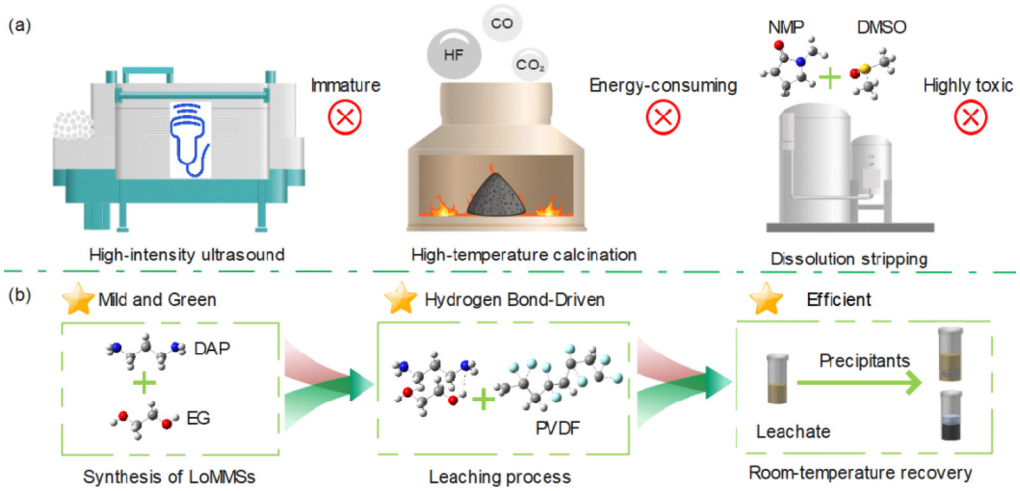

Fig. 1 A comparison between the traditional approach (a) and the hydrogen bond-driven strategy for PVDF recovery proposed in this work (b).

Herein, for the first time, we propose a hydrogen bond-driven strategy with ultrasonic assistance for ultrafast and eco-friendly recovery of PVDF nanoplastic from polymer solid electrolytes using LoMMSs (Fig. 1). LoMMSs are not restricted by the eutectic melting point and can thus be regarded as an expansion and extension of DESs.[35] By leveraging the synergistic effects of hydrogen bond network regulation in green solvents and ultrasonic-induced cavitation, this strategy achieves efficient breakdown of C–F bonds in PVDF, thereby facilitating rapid and enhanced leaching of PVDF nanoplastic from spent polymer solid electrolytes.

2. Materials and methods

2.1. Materials

All reagents and materials used in the experiment were commercially available and not further purified. Nanoscale PVDF powder (99%, 800 nm size, Dongguan Jiaxin Plastic Raw Material Co., Ltd), 1,3-diaminopropane (DAP, 98%, Shandong Keyuan Biochemical Co., Ltd), ethylene glycol (EG, 98%, Shanghai Aladdin Biochemical Technology Co., Ltd), polyethylene glycol 200 (PEG 200, ≥95%, Tianjin Bairuns Biotechnology Co., Ltd), glycerol (≥99.0%, Tianjin Fuyu Fine Chemical Co., Ltd), glacial acetic acid (GAA, 99.5%, Shanghai Aladdin Biochemical Technology Co., Ltd), hydrobromic acid (HBr, 40%, Shanghai Aladdin Biochemical Technology Co., Ltd), phosphoric acid (H_3PO_4, ≥85.0%, Sinopharm Chemical Reagent Co., Ltd), hydrochloric acid (HCl, 37%, Tianjin Zhiyuan Chemical Reagent Co., Ltd), sulfuric acid (H_2SO_4, 98%, Tianjin Zhiyuan Chemical Reagent Co., Ltd), nitric acid (HNO_3, 68%, Tianjin Damao Chemical Reagent Co., Ltd), oxalic acid (OA, ≥99.5%, Tianjin Chemical Reagent Supply and Marketing Co., Ltd), and deionized water (laboratory-made) were used in this study.

2.2. Synthesis and leaching

DAP and EG were mixed in a certain molar ratio in a glass bottle under vigorous shaking to prepare the LoMMSs. Then, PVDF nanoplastic was added to the LoMMSs, and the mixture was treated using a KQ-500B ultrasonic cleaner under certain conditions. Then the mixture was centrifuged, and the supernatant was collected as the leachate. Physical property analysis included the measurement of density, viscosity, and conductivity, with each being measured several times. Subsequently, 250 μL of the leachate was diluted with deionized water at a volume ratio of 1 : 200. The millivoltage of the diluted solution was measured using a PXSJ-216F F ion-selective electrode, and the F ion leaching efficiency was calculated using eqn (1), where η_x is the leaching efficiency of F, c is the concentration of F in the leaching solution, m and ρ are the mass and density of LoMMSs, and M_x is the relative molecular mass of F in PVDF.

$$\eta_x = \frac{cm/\rho}{M_x} \times 100\% \quad (1)$$

2.3. Precipitation

Precipitants were utilized for the recovery of the leachate, where the leachate was prepared under the following conditions: 5 g of LoMMSs, 0.1 g of PVDF nanoplastic, a temperature of 80 °C, and an ultrasonic treatment duration of 1.5 h. A total of 37 precipitants covering different polarity and hydrogen bond donor/acceptor ability were tested for leachate recovery at room temperature. Firstly, 2 mL of the leachate and 2 mL of each precipitant were added to a centrifuge tube. Subsequently, the centrifuge tube containing the precipitants and leachate was sonicated for 40 min, then allowed to stand for precipitation for 2 days, yielding three types of precipitation results: (1) liquid + solid phases; (2) homogeneous liquid phase; and (3) liquid + liquid phases.

3. Results and discussion

3.1. Effect of hydrogen bond donors

Three types of hydrogen bond donors including EG, PEG200 and Gly with the hydrogen acceptor DAP are synthesized and

the solubility of the systems is investigated at room temperature and 80 °C. DAP can form homogenous liquids as LoMMSs with EG, PEG200 or Gly. Then, 5 g of LoMMSs are mixed with 0.1 g of PVDF and subjected to ultrasonic stirring for 30 min at 80 °C. The F leaching efficiencies from PVDF nanoplastic are in the following order: EG-based leachate (68.8%) > PEG200-based leachate (25.2%) > Gly-based leachate (23.8%) (Fig. 2a and Table 1). Therefore, DAP : EG exhibits a better leaching ability. Compared with PEG200 or Gly, EG features a smaller molecular configuration and lower viscosity, which facilitates hydrogen bond-induced interactions with PVDF and thus promotes the F leaching efficiency.

3.2. Effect of the molar ratio of DAP : EG in LoMMSs

Under the conditions of 80 °C and ultrasonic treatment for 30 min, the F leaching efficiency from PVDF nanoplastic decreases as the molar ratio of DAP : EG increases from 1 : 1 to 4 : 1 (Fig. 2b and Table 1). The corresponding F leaching efficiencies are 68.7%, 41.1%, 21.0% and 14.6%, respectively. The possible reason is that the concentration of $-NH_2$ groups in the system drops significantly as the concentration of DAP decreases. This directly reduces the collision probability between $-NH_2$ groups and C–F bonds on PVDF molecular chains, making it difficult for nucleophilic reactions to proceed efficiently and thus significantly lowering the F dissociation efficiency. Therefore, an appropriate DAP : EG molar ratio of 1 : 1 is determined for F leaching from PVDF.

3.3. Effect of temperature

Temperatures of 25 °C, 40 °C, 60 °C and 80 °C are selected for the leaching of F from PVDF nanoplastic using LoMMSs. The results indicate that the leaching efficiency increases with temperature when the time period is kept constant (Fig. 3a–e).

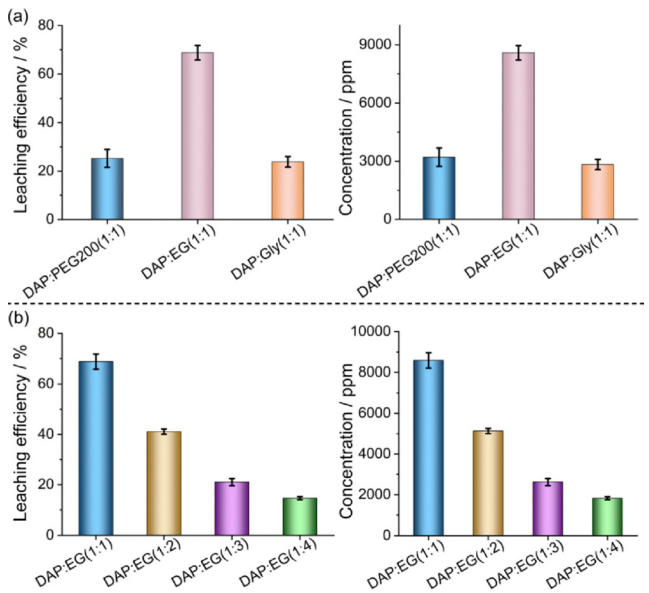

Fig. 2 Effect of hydrogen bond donors (a) and the molar ratio (b) on the F leaching efficiency and concentration from PVDF nanoplastic in polymer solid electrolytes of ASLIBs.

Table 1 Factors influencing the leaching efficiency and concentration of F from PVDF nanoplastic in polymer solid electrolytes of ASLIBs

Factors	Value	cF (ppm)	ηF (%)
LoMMSs	DAP : PEG200 (1 : 1)	3209.3 ± 473.7	25.2 ± 3.7
	DAP : EG (1 : 1)	8583.8 ± 377.3	68.7 ± 3.0
	DAP : Gly (1 : 1)	2831.5 ± 260.8	23.8 ± 2.1
Molar ratio	DAP : EG (1 : 1)	8583.8 ± 377.3	68.7 ± 3.0
	DAP : EG (1 : 2)	5130.9 ± 127.1	41.1 ± 1.0
	DAP : EG (1 : 3)	2625.4 ± 175.2	21.0 ± 1.4
	DAP : EG (1 : 4)	1826.8 ± 75.3	14.6 ± 0.6
Time (h), 25 °C	0.17	2085.1 ± 96.8	16.7 ± 0.7
	0.5	2230.7 ± 89.9	17.8 ± 0.7
	1	2325.0 ± 43.1	18.6 ± 0.3
	1.5	2463.3 ± 186.5	19.7 ± 1.4
	2	2532.4 ± 231.5	20.2 ± 1.7
Time (h), 40 °C	0.17	2017.9 ± 54.5	16.1 ± 0.4
	0.5	2048.3 ± 46.4	16.4 ± 0.3
	1	2153.8 ± 62.3	17.2 ± 0.4
	1.5	2709.8 ± 67.3	21.7 ± 0.5
	2	2894.9 ± 43.4	23.1 ± 0.3
Time (h), 60 °C	0.17	4008.7 ± 230.7	32.1 ± 1.6
	0.5	4504.5 ± 230.7	36.0 ± 1.8
	1	5601.2 ± 275.3	44.8 ± 2.2
	1.5	7842.5 ± 35.3	65.7 ± 0.2
	2	10 215.1 ± 264.4	81.9 ± 2.1
Time (h), 80 °C	0.17	6067.6 ± 341.0	48.6 ± 2.7
	0.5	8583.8 ± 377.3	68.7 ± 3.0
	1	9482.2 ± 509.7	75.9 ± 4.0
	1.5	11 086.5 ± 324.6	88.8 ± 2.6
	2	11 424.5 ± 292.9	91.5 ± 2.3
LoMMS mass (g)	5	11 086.5 ± 324.6	88.8 ± 2.6
	10	5683.5 ± 56.2	91.1 ± 0.9
	15	4056.1 ± 94.2	97.5 ± 2.3
	20	3063.1 ± 30.8	98.2 ± 1.0

For instance, at a fixed leaching time of 0.17 h, the F leaching efficiency increases with increasing temperature from 25 °C to 80 °C, achieving values of 16.7%, 16.1%, 32.1%, and 48.6% (Fig. 3a). Therefore, 80 °C is selected as the leaching temperature for further investigation. Moreover, changes in temperature have little effect on the F leaching efficiency below 40 °C, while the F leaching efficiency increases significantly above 40 °C (Fig. 3a–e). A possible reason might be that LoMMSs cannot effectively penetrate the PVDF matrix or activate the C–F bonds below 40 °C, leading to a relatively low leaching efficiency; in contrast, the supplied thermal energy is sufficient to meet the energy requirement for C–F bond cleavage in the hydrogen bond network when the temperature exceeds 40 °C.

3.4. Effect of time

The effect of time varying from 0.17 h (10 min) to 2 h on leaching efficiency is investigated under the condition of DAP : EG = 1 : 1. The F leaching efficiency from PVDF nanoplastic increases with time at all the temperatures investigated (Fig. 4a). For example, the F leaching efficiencies at 80 °C are 48.6%, 68.8%, 76.0%, 88.8% and 91.5% at 0.17 h, 0.5 h, 1 h, 1.5 h and 2 h, respectively. Kinetic models for the leaching process are investigated. Fig. 4b shows that the data fit with the diffusion-controlled model,[48] surface reaction-controlled model, and Avrami model. The R^2 values for the diffusion-controlled model (0.98), the Avrami model (0.94), and the surface reaction-controlled model (0.88) are all relatively high,

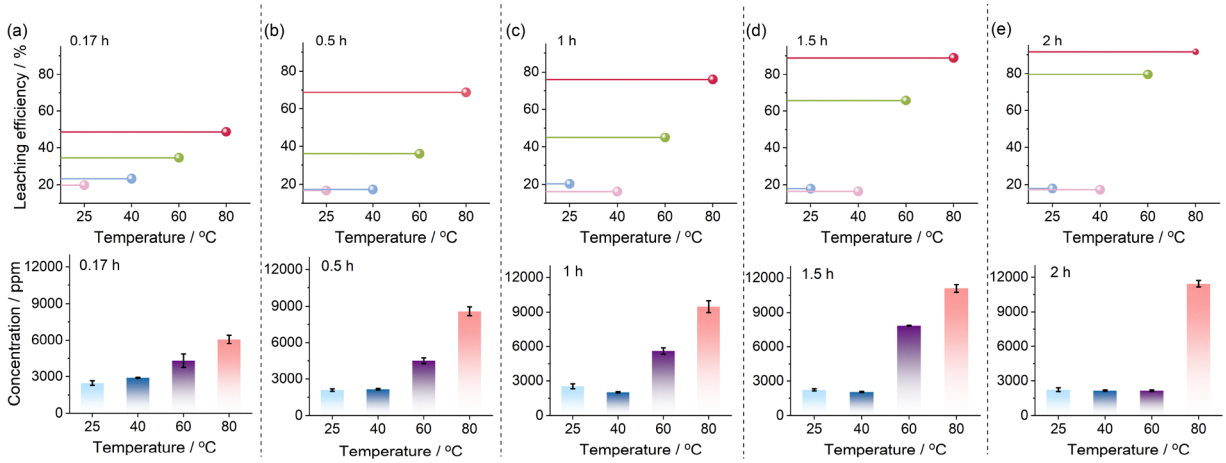

Fig. 3 Effect of temperature on the F leaching efficiency and concentration from PVDF nanoplastic in polymer solid electrolytes of ASLIBs at 0.17 h (a), 0.5 h (b), 1 h (c), 1.5 h (d) and 2 h (e).

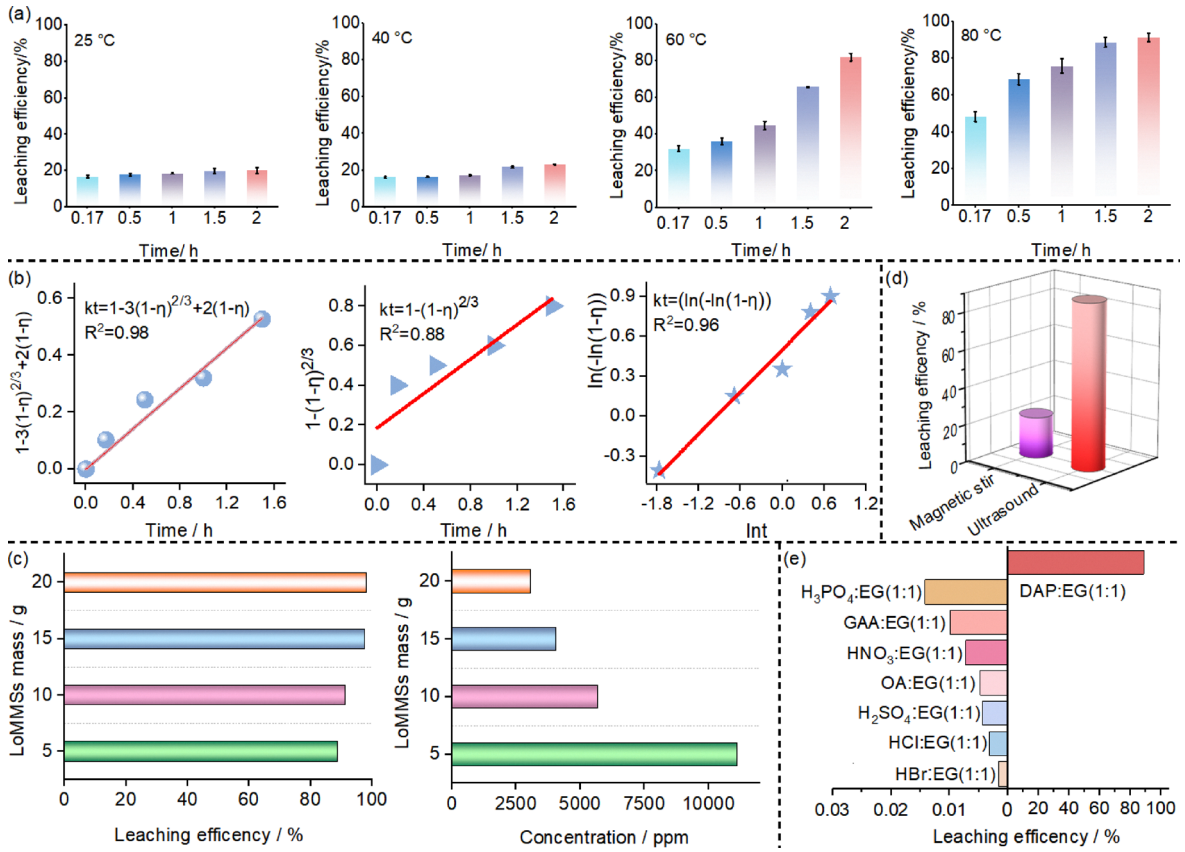

Fig. 4 (a) Effect of time on the F leaching efficiency from PVDF nanoplastic at different temperatures; (b) kinetic regression using the diffusion-controlled model $kt = 1 - 3(1-\eta)^{2/3} + 2(1-\eta)$, the surface reaction-controlled model $kt = 1-(1-\eta)^{2/3}$, and the Avrami kinetic model $kt = \ln(-\ln(1-\eta))$; (c) effect of the solid–liquid ratio; (d) comparison between magnetic stirring and ultrasonic treatment; and (e) effects of different solvent systems.

suggesting that the leaching process likely results from the synergistic effects of multiple kinetic factors.

3.5. Effect of the liquid-to-solid ratio (L/S)

With the leaching temperature fixed at 80 °C and ultrasonic time at 0.17 h, the effect of L/S mass ratios (50, 100, 150, and 200 corresponding to LoMMS masses of 5 g, 10 g, 15 g and 20 g) on the leaching of PVDF nanoplastic is investigated. Fig. 4c shows that as the L/S ratio increases from 50 to 200, the F leaching efficiency exhibits a continuous upward trend, gradually increasing from 88.8% to 98.2%. There is a significant correlation between the L/S ratio and the F leaching efficiency

from PVDF in the leaching system. Particularly, the higher the L/S ratio, the higher the F leaching efficiency. However, the concentration of F decreases with increasing L/S ratio. Therefore, 50 is the preferred L/S ratio.

3.6. Effect of ultrasonic treatment

Ultrasonic treatment is compared with magnetic stirring in terms of its influence on F leaching efficiency from PVDF nanoplastic. It can be seen that the F leaching efficiency in the system assisted by ultrasonic treatment reaches 88.8% within 1.5 h, approximately 67% higher than that 21.7% achieved with magnetic stirring (Fig. 4d). This can be explained by the fact that ultrasonic treatment can effectively enhance the mutual penetration between LoMMSs and PVDF, accelerate molecular diffusion and collision frequency in the system, and improve leaching efficiency, while magnetic stirring relies solely on physical mixing, which fails to better promote the mutual penetration between LoMMSs and PVDF, making it difficult to achieve an enhancement in leaching efficiency.

3.7. Comparison of solvent systems

Under the conditions of 80 °C and an ultrasonic treatment duration of 1.5 h, the effects of eight different solvent systems on the F leaching efficiency from PVDF nanoplastic are investigated. These eight solvents all consist of the same hydrogen bond donor (*i.e.*, EG) combined with one of the following hydrogen bond acceptors: DAP, GAA, HNO_3, OA, H_2SO_4, H_3PO_4, HCl, and HBr. As shown in Fig. 4e and Table S1, DAP : EG exhibits the highest F leaching efficiency among all eight solvent systems investigated. The F leaching efficiency is ranked as follows: DAP : EG (88.8%) $\gg$ H_3PO_4 : EG (0.0141%) > GAA : EG (0.0099%) > HNO_3 : EG (0.0072%) > OA : EG (0.0047%) > H_2SO_4 : EG (0.0043%) > HCl : EG (0.0032%) > HBr : EG (0.0016%). It can be concluded that the alkaline DAP : EG system efficiently leaches F from PVDF nanoplastic, whereas the other acidic systems exhibit only negligible F leaching efficiency.

3.8. Physical properties and mechanism

As shown in Fig. 5a, the density follows the order: EG (1.1107 g cm^3) > leachate (1.0037 g cm^3) > LoMMSs (1.001 g cm^3) > DAP (0.8787 g cm^3). The electrical conductivity of the leachate (477.75 μS cm^{-1}) is significantly higher than those of LoMMSs (20.38 μS cm^{-1}), DAP (2.11 μS cm^{-1}) and EG (0.73 μS cm^{-1}). This indicates that the degradation of PVDF in the leachate produces a large number of mobile F-containing ions, leading to a sharp increase in F concentration and a direct increase in electrical conductivity. The order of viscosity is determined as: LoMMSs (36.06 mPa s) > leachate (33.48 mPa s) > EG (20.48 mPa s) > DAP (6.04 mPa s). The higher viscosity of LoMMSs compared to EG and DAP can be attributed to the stable intermolecular hydrogen-bonding network formed between EG and DAP. After PVDF leaching, this hydrogen-bonding network in LoMMSs is disrupted, resulting in a significantly lower viscosity of the leachate than that of the original LoMMSs.

In the IR spectra (Fig. 5b), the characteristic C–F stretching peaks (1000–1400 cm^{-1}) of pristine PVDF completely disappear in the leaching residue, while they appear prominently in the leachate. This indicates that all F-containing groups from PVDF are released into the leachate, leaving no detectable F in the residue. Notably, the IR spectra of LoMMSs show no obvious C–F stretching peaks (1000–1400 cm^{-1}), confirming that the F-containing groups detected in the leachate originate exclusively from PVDF. The IR spectra of LoMMSs and the resulting leachate exhibit highly similar absorption patterns, indicating excellent stability of the LoMMSs during the leaching process. The peak shapes of LoMMSs differ from that of either DAP or EG, confirming the formation of hydrogen bonds between EG and DAP. The ^1H and ^{13}C NMR spectra (Fig. 5c) of LoMMSs and the leachate show only minor shifts, which align with the IR spectra and further support the stability of LoMMSs.

Both magnetic stirring (Fig. 6a) and ultrasonic treatment (Fig. 6b) share the same fundamental mechanism of F leaching from PVDF nanoplastic, but ultrasonic treatment additionally provides high energy that actively destroys and degrades the PVDF nanoplastic structure. EG serves as a dual-functional solvent in this system and its interaction with PVDF proceeds through a multi-step mechanism. First, EG not only swells the PVDF matrix but also disperses DAP, thereby facilitating the deep penetration of LoMMSs into the internal structure of PVDF *via* ultrasonic treatment. Then, EG, as a hydrogen bond donor, forms intermolecular hydrogen bonds with DAP, which effectively enhance the dispersion stability of the LoMMS system. Meanwhile, EG establishes weak hydrogen bond interactions with the F atoms in PVDF molecules. This interaction reduces the bond energy of the C–F bonds in PVDF, rendering them susceptible to nucleophilic attack by the nitrogen atoms in the LoMMSs. Subsequent cleavage of the activated C–F bonds occurs, followed by the formation of N–F bonds between the released F atoms and nitrogen atoms. This hydrogen bond-driven process—from matrix swelling and solvent penetration to hydrogen bond-induced bond activation and cleavage—ultimately achieves efficient F leaching from PVDF. It can be analogized to flower roots (*i.e.*, solvents) penetrating dense rock (*i.e.*, PVDF nanoplastic), as shown in Fig. 6c.

3.9. Precipitation from leachate

As shown in Fig. 7a, distinct precipitation occurs with five precipitants (*i.e.*, tetrabutyl titanate (TBT), acetic acid (ACA), levulinic acid (LevA), dichloromethane (DCM), and calcium hydroxide ($Ca(OH)_2$)), resulting in a liquid–solid two-phase system. The precipitates formed by these five precipitants exhibit typical crystalline morphology, which provides preliminary evidence for their potential in selective metal recovery from the LoMMS-based leachate system. In contrast, no visible precipitation occurs with the other 32 precipitants, which instead form a liquid + liquid two-phase system (Fig. 7b) or a single homogeneous liquid phase (Fig. 7c). The six precipitants that show liquid–liquid two-phase behavior include triethylamine (TEA), methyl *tert*-butyl ether (MTBE), malononitrile (MN), engine oil (ENO), polydimethylsiloxane (PDMS), and

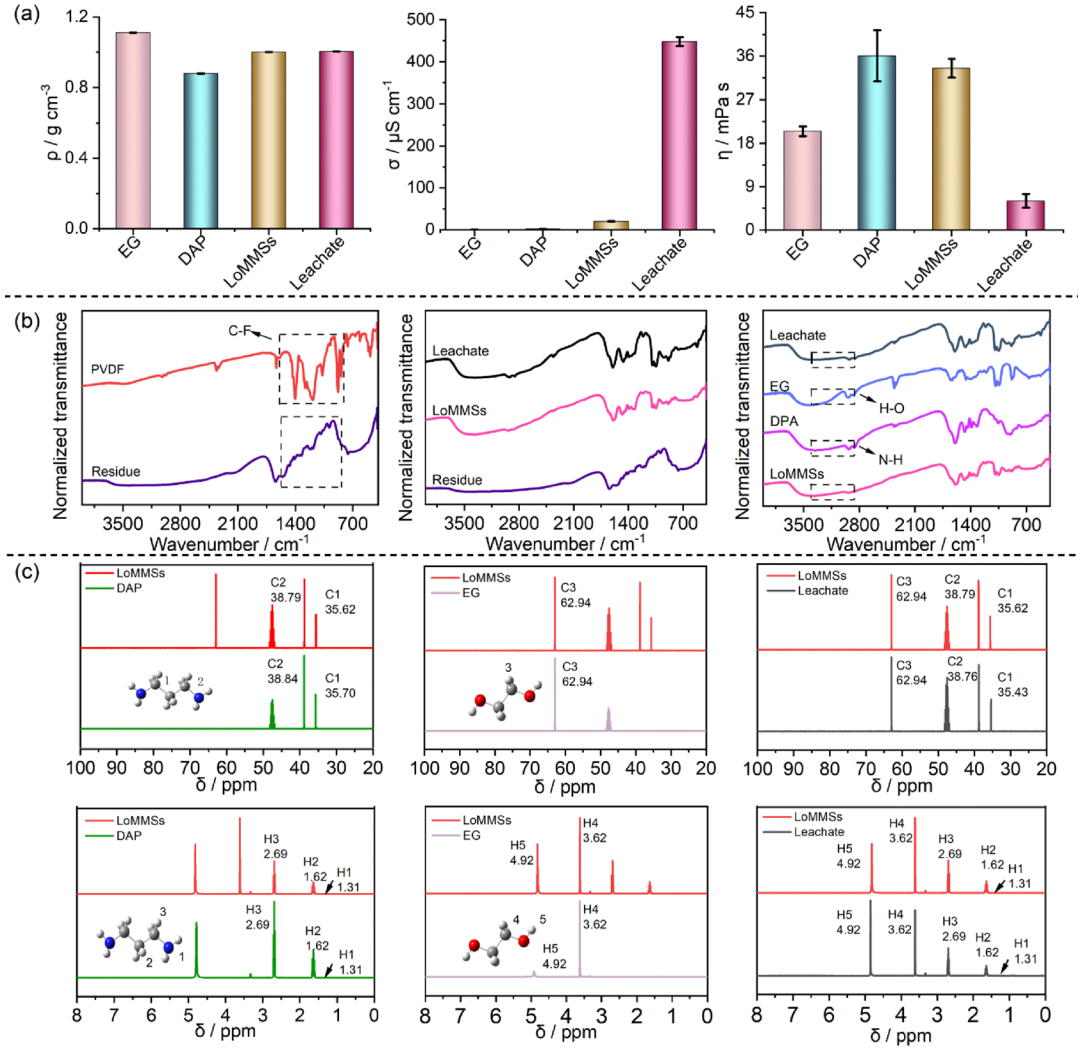

Fig. 5 Density, electrical conductivity, and viscosity (a) of EG, DAP, LoMMSs and leachate; comparison of the IR spectra (b) and NMR spectra (c) of EG, DAP, LoMMSs, residue, and leachate.

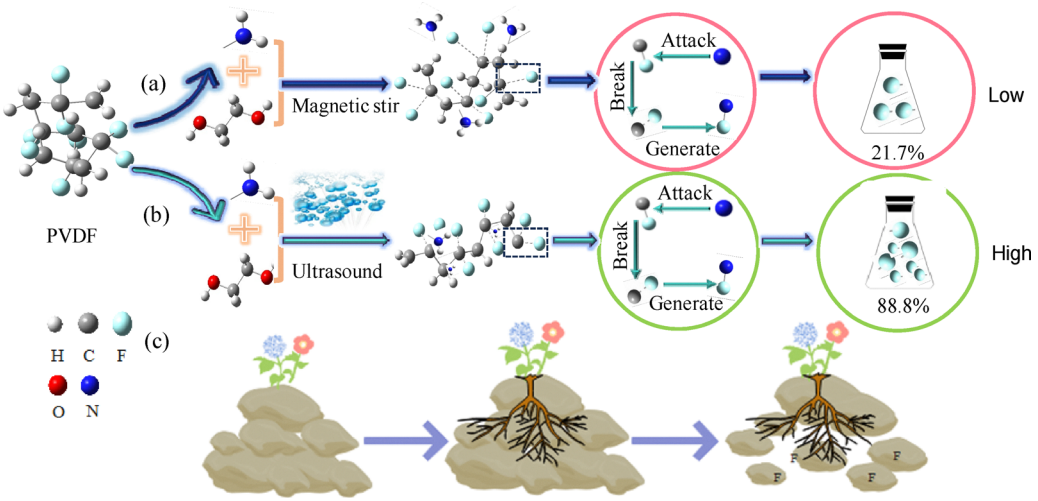

Fig. 6 Proposed mechanism of F leaching from PVDF nanoplastic using LoMMSs under magnetic stirring (a) and ultrasound treatment (b); (c) the analogous process of C–F bond cleavage.

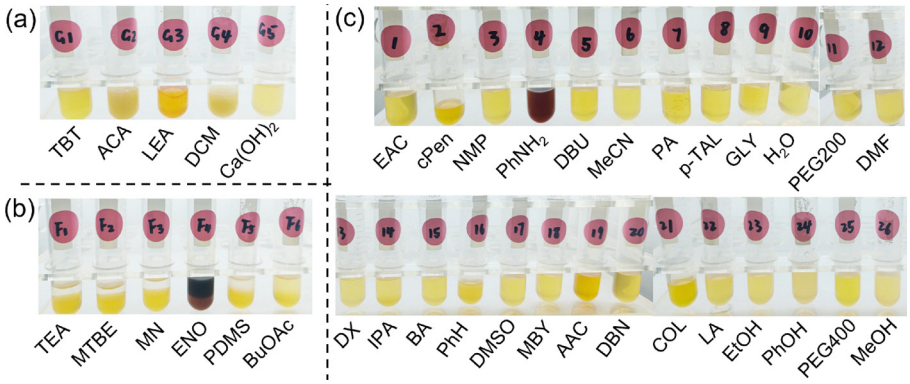

Fig. 7 Precipitation of PVDF from the leachate by forming liquid + solid phases (a), liquid + liquid phases (b), and a single homogeneous liquid phase (c).

N-butyl acetate (BuOAc). A total of 26 precipitants exhibiting a single homogeneous liquid phase are ethyl acetate (EAC), cyclopentane (cPen), *N*-methylpyrrolidone (NMP), aniline ($PhNH_2$), 1,8-diazabicyclo[5,4,0]undec-7-ene (DBU), acetonitrile (MeCN), propanoic acid (PA), 4-methylbenzaldehyde (*p*-TAL), glycerol (GLY), water (H_2O), polyethylene glycol 200 (PEG200), *N*,*N*-dimethylformamide (DMF), 1,4-dioxane (DX), isopropanol (IPA), benzoic acid (BA), benzene (PhH), dimethyl sulfoxide (DMSO), 2-methylbut-3-yn-2-ol (MBY), acetylacetone (AAC), 1,5-diazabicyclo[4.3.0]non-5-ene (DBN), collodion (COL), lactic acid (LA), ethanol (EtOH), phenol (PhOH), polyethylene glycol 400 (PEG400), and methyl alcohol (MeOH).

3.10. Comparison

The five PVDF recycling methods are compared in terms of the F leaching efficiency, required operating conditions, solvent recyclability, and key disadvantages (Table S2). The high-intensity ultrasonication method achieves over 82% F removal under the conditions of 25 kHz, 998–1002 W, and 12 h, but its removal process is immature and difficult to industrialize.[49] High-temperature calcination yields an F removal efficiency of 85–95% at 400–600 °C, but generates toxic HF gas emission.[50–52] Dissolution stripping with NMP + DMSO reaches over 90% removal after refluxing at 200 °C for 24 h, though the solvents are highly toxic (harmful to humans and the environment) and solution recovery is complex.[53,54] Fluid extraction using CO_2 + DMSO achieves a high F removal efficiency of 98.5% under the conditions of 70 °C, 80 bar and 13 min, with recyclable and zero-loss solvents, but requires complex and corrosion-resistant equipment.[55] The LoMMSs of DAP : EG developed *via* the hydrogen bond-driven strategy in this work achieves 98.2% F removal after optimization, featuring green and recyclable solvents without significant disadvantages.

4. Conclusions

In summary, a hydrogen bond-driven strategy for the efficient recovery of PVDF nanoplastic from polymer solid electrolytes of ASLIBs is proposed. By integrating LoMMSs of DAP : EG, hydrogen bond network regulation, and ultrasonic treatment, the proposed strategy achieves the highest F leaching efficiency of 98.2% after proper optimization. Under comparable conditions, the F leaching efficiency achieved through the hydrogen-bond driven strategy with ultrasound assistance is nearly 88% greater than that of traditional solvent methods and approximately 67% more effective than that of magnetic stirring processes. The hydrogen bond network regulation through an ultrasonic induced cavitation mechanism is illustrated. Therefore, it not only provides a novel, rapid, and eco-friendly strategy for the recycling of spent PVDF nanoplastic from polymer solid electrolytes, but also offers valuable insights into the design of hydrogen bond-driven processes for plastic recovery. Future work may focus on extending the application scope of this hydrogen bond-driven strategy to the recovery of other composites from polymer solid electrolytes of ASLIBs.

Author contributions

Xuemin Jing: conceptualization, supervision, writing – original draft, writing – review & editing, project administration, funding acquisition. Qianqian Liu, Xingyu Shi, Ziyi Sun, Zhenghui Liu, Zhenyang Li and Na Ni: investigation, data curation. Yu Chen: conceptualization, supervision, writing – original draft, writing – review & editing, project administration, funding acquisition.

Conflicts of interest

The authors declare no competing financial interests.

Data availability

The data (including leaching F from PVDF nanoplastic and comparison of five PVDF recycling methods) that support the findings of this study are available upon reasonable request. Requests to access these data should be directed to yuchen@iccas.ac.cn.

The data supporting this article have been included as part of the supplementary information (SI). Supplementary information is available. See DOI: https://doi.org/10.1039/d5cp05042a.

Acknowledgements

This work was supported by the National Natural Science Foundation of China (22103030), the Natural Science Foundation of Hebei Province/S&T Program of Hebei (B2024408022), the Start-up Fund for Doctoral Research of Langfang Normal University (XBQ202046), and the Fundamental Research Funds for the Universities in Hebei Province (JYT202502).

References

1 Y. Guo, J. Zhao, L. Liu, X. Cai, H. Shi, F. Zhang, J. Xu and X. Wu, Lithium aluminum titanium phosphate (LATP) composite solid-state electrolytes: progress and prospects for all-solid-state batteries, *Nanoscale*, 2025, **17**, 26642–26657.

2 B. Yuan, G. Wang, T. Zhao and Y. Liang, A multifunctional aramid-reinforced PVDF solid electrolyte for thermally robust lithium metal battery, *Mater. Today Energy*, 2025, **54**, 102115.

3 A. Manthiram, X. Yu and S. Wang, Lithium battery chemistries enabled by solid-state electrolytes, *Nat. Rev. Mater.*, 2017, **2**, 16103.

4 Z. Fang, M. Zhao, Y. Peng and S. Guan, Combining Organic Plastic Salts with a Bicontinuous Electrospun PVDF–HFP/$Li_7La_3Zr_2O_{12}$ Membrane: LiF-Rich Solid-Electrolyte Interphase Enabling Stable Solid-State Lithium Metal Batteries, *ACS Appl. Mater. Interfaces*, 2022, **14**, 18922–18934.

5 Z. Su, Z. Yuan, W. He, L. Zhang and Z. Cheng, PVDF-Based Salt-Concentrated Polymer Electrolyte with High Intrinsic Lithium Salt Dissociation Capability and Ionic Conductivity, *Ind. Eng. Chem. Res.*, 2025, **64**, 21329–21337.

6 J. Li, W. Zheng, L. Zhu, H. Zhou and K. Zhang, Incorporating lithium magnesium silicate into PVDF-HFP based solid electrolyte to achieve advanced solid-state lithium-ion batteries, *J. Alloys Compd.*, 2023, **960**, 170640.

7 J. Speirs, M. Contestabile, Y. Houari and R. Gross, The future of lithium availability for electric vehicle batteries, *Renewable Sustainable Energy Rev.*, 2014, **35**, 183–193.

8 M. Wang, K. Liu, J. Yu, Q. Zhang, Y. Zhang, M. Valix and D. C. W. Tsang, Challenges in Recycling Spent Lithium-Ion Batteries: Spotlight on Polyvinylidene Fluoride Removal, *Global Challenges*, 2023, **7**, 2200237.

9 P. Danz, V. Aryan, E. Möhle and N. Nowara, Experimental Study on Fluorine Release from Photovoltaic Backsheet Materials Containing PVF and PVDF during Pyrolysis and Incineration in a Technical Lab-Scale Reactor at Various Temperatures, *Toxics*, 2019, **7**, 47.

10 A. Li, Z. Sun, C. Lv and Z. Fu, Recent progress in removal and recovery of PVDF from spent lithium-ion batteries, *Sep. Purif. Technol.*, 2026, **380**, 135193.

11 Y. Ji, C. T. Jafvert, N. N. Zyaykina and F. Zhao, Decomposition of PVDF to delaminate cathode materials from end-of-life lithium-ion battery cathodes, *J. Cleaner Prod.*, 2022, **367**, 133112.

12 F. M. Perna, P. Vitale and V. Capriati, Deep eutectic solvents and their applications as green solvents, *Curr. Opin. Green Sustainable Chem.*, 2020, **21**, 27–33.

13 D. Yu, D. Jiang, Z. Xue and T. Mu, Deep eutectic solvents as green solvents for materials preparation, *Green Chem.*, 2024, **26**, 7478–7507.

14 J. Liu, X. Li and K. H. Row, Development of deep eutectic solvents for sustainable chemistry, *J. Mol. Liq.*, 2022, **362**, 119654.

15 J. K. U. Ling and K. Hadinoto, Deep Eutectic Solvent as Green Solvent in Extraction of Biological Macromolecules: A Review, *Int. J. Mol. Sci.*, 2022, **23**, 3381.

16 X. Ge, C. Gu, X. Wang and J. Tu, Deep eutectic solvents (DESs)-derived advanced functional materials for energy and environmental applications: challenges, opportunities, and future vision, *J. Mater. Chem. A*, 2017, **5**, 8209–8229.

17 S. Zhang, J. Sun, X. Zhang, J. Xin, Q. Miao and J. Wang, Ionic liquid-based green processes for energy production, *Chem. Soc. Rev.*, 2014, **43**, 7838–7869.

18 X. Zhang, X. Fan, H. Niu and J. Wang, An ionic liquid as a recyclable medium for the green preparation of α,α′-bis (substituted benzylidene)cycloalkanones catalyzed by $FeCl_3{\cdot}6H_2O$, *Green Chem.*, 2003, **5**, 267–269.

19 K. Yu, W. Ding, Y. Lu, Y. Wang, Y. Liu, G. Liu, F. Huo and H. He, Ionic liquids screening for lignin dissolution: COSMO-RS simulations and experimental characterization, *J. Mol. Liq.*, 2022, **348**, 118007.

20 W. Ding, W. Zhu, J. Xiong, L. Yang, A. Wei, M. Zhang and H. Li, Novel heterogeneous iron-based redox ionic liquid supported on SBA-15 for deep oxidative desulfurization of fuels, *Chem. Eng. J.*, 2015, **266**, 213–221.

21 J. Liu, Y. Wang, B. Gao, K. Zhang, H. Li, J. Ren, F. Huo, B. Zhao, L. Zhang, S. Zhang and H. He, Ionic Liquid Gating Induces Anomalous Permeation through Membrane Channel Proteins, *J. Am. Chem. Soc.*, 2024, **146**, 13588–13597.

22 W. Zhao, Z. Xue, J. Wang, J. Jiang, X. Zhao and T. Mu, Large-Scale, Highly Efficient, and Green Liquid-Exfoliation of Black Phosphorus in Ionic Liquids, *ACS Appl. Mater. Interfaces*, 2015, **7**, 27608–27612.

23 Y. Zhou, Y. Zheng, T. Zhang, G. Deng and Z. Yu, Evidence that Acetonitrile is Sensitive to Different Interaction Sites of Ionic Liquids as Revealed by Excess Spectroscopy, *Chem. Phys. Chem.*, 2017, **18**, 1370–1375.

24 X. Pi, J. Lu, S. Li, J. Zhang, Y. Wang and H. He, Computer-aided ionic liquid design for green chemical processes based on molecular simulation and artificial intelligence, *Sep. Purif. Technol.*, 2025, **361**, 131585.

25 K. Li, Y. Wang, C. Wang, F. Huo, S. Zhang and H. He, Fluorine Domains Induced Ultrahigh Nitrogen Solubility in Ionic Liquids, *J. Am. Chem. Soc.*, 2024, **146**, 25569–25577.

26 J. Lu, T. Sun, Y. Lu, H. He and Y. Wang, Weakening origin of hydrogen bond in ionic liquid at the electrified interface, *AIChE J.*, 2025, **71**, e18660.

27 G. Brunner, Applications of Supercritical Fluids, *Annu. Rev. Chem. Biomol. Eng.*, 2010, **1**, 321–342.

28 Ž. Knez, E. Markočič, M. Leitgeb, M. Primožič, M. Knez Hrnčič and M. Škerget, Industrial applications of supercritical fluids: A review, *Energy*, 2014, **77**, 235–243.

29 P. Pollet, C. A. Eckert and C. L. Liotta, Switchable solvents, *Chem. Sci.*, 2011, **2**, 609–614.
30 P. G. Jessop, S. M. Mercer and D. J. Heldebrant, CO_2-triggered switchable solvents, surfactants, and other materials, *Energy Environ. Sci.*, 2012, **5**, 7240–7253.
31 D. Yu and T. Mu, Strategy To Form Eutectic Molecular Liquids Based on Noncovalent Interactions, *J. Phys. Chem. B*, 2019, **123**, 4958–4966.
32 H. Malaeke, M. R. Housaindokht, H. Monhemi and M. Izadyar, Deep eutectic solvent as an efficient molecular liquid for lignin solubilization and wood delignification, *J. Mol. Liq.*, 2018, **263**, 193–199.
33 Q. Liu, H. Mou, W. Chen, X. Zhao, H. Yu, Z. Xue and T. Mu, Highly Efficient Dissolution of Lignin by Eutectic Molecular Liquids, *Ind. Eng. Chem. Res.*, 2019, **58**, 23438–23444.
34 D. Yu, Z. Xue and T. Mu, Eutectics: formation, properties, and applications, *Chem. Soc. Rev.*, 2021, **50**, 8596–8638.
35 Y. Chen and Z. Yu, Low-melting mixture solvents: extension of deep eutectic solvents and ionic liquids for broadening green solvents and green chemistry, *Green Chem. Eng.*, 2024, **5**, 409–417.
36 X. Huang, W. Dong, X. Luo, L. Xu, D. Yang and Y. Wang, Low-melting mixture solvents as novel solubilizing agents: Improving tolvaptan formulation and therapeutic efficacy, *J. Mol. Liq.*, 2024, **414**, 126179.
37 Y. Chen, F. Zhang, Y. Chang, J. Wang, Q. Zhang, M. Yang, Z. Liu and Z. Zhang, Natural Biomass Soups (NBSs): New Green Solvents Replacing Ionic Liquids and Deep Eutectic Solvents for Lithium-Ion Batteries Recovery, *Energy Fuels*, 2023, **37**, 19076–19081.
38 J. Fernández-López, C. Botella-Martínez, C. Navarro-Rodríguez de Vera, M. E. Sayas-Barberá, M. Viuda-Martos, E. Sánchez-Zapata and J. A. Pérez-Álvarez, Vegetable Soups and Creams: Raw Materials, Processing, Health Benefits, and Innovation Trends, *Plants*, 2020, **9**, 1769.
39 Y. Chen, Z. Yang, Y. Wang, G. Zhao, T. Wang, M. Feng, M. Zhao, X. Wang and D. Dong, Biomass-based vegetable-/fruit-derived solvents for green recovery of $LiFePO_4$ cathodes from spent lithium-ion batteries: alternatives to ionic liquids, deep eutectic solvents and low-melting mixture solvents, *New J. Chem.*, 2025, **49**, 11985–11995.
40 Y. Chen, F. Zhang, H. Sun, Y. Chang, Z. Zhang, Z. Liu and M. Yang, Superlong supercooling solvents (SSSs): Alternative green solvents to ionic liquids and deep eutectic solvents for lithium-ion batteries recycling, *J. Mol. Liq.*, 2023, **391**, 123410.
41 M. A. Anisimov, Cold and supercooled water: A novel supercritical-fluid solvent, *Russ. J. Phys. Chem. B*, 2012, **6**, 861–867.
42 N. V. Medhekar, A. Ramasubramaniam, R. S. Ruoff and V. B. Shenoy, Hydrogen Bond Networks in Graphene Oxide Composite Paper: Structure and Mechanical Properties, *ACS Nano*, 2010, **4**, 2300–2306.
43 R. Wang, M. DelloStritto, M. L. Klein, E. Borguet and V. Carnevale, Topological properties of interfacial hydrogen bond networks, *Phys. Rev. B*, 2024, **110**, 014105.
44 A. Zeng, D. Zeng, Y. Luo, X. Qv, H. Zhao, X. Feng, P. Chen, Z. Wang, Y. Wu and K. Guo, Weakly coordinated TGDE regulating hydrogen bond network and solvated structure for high-rate Zn anodes, *J. Energy Chem.*, 2026, **113**, 811–820.
45 X. Kong, D. Li, C. Feng, X. Zhao, H. Chen, Z. Cao and Y. Gu, Hydrogen Bonding Networks in Hybrid Binders Inhibit Vanadium Dissolution for Stable Aqueous Zinc-Ion Batteries, *Langmuir*, 2025, **41**, 30360–30369.
46 A. Ali, A. Ali, A. Tahir, M. A. Bakht and M. J. Ahsan, Ultrasound promoted green synthesis, anticancer evaluation, and molecular docking studies of hydrazines: a pilot trial, *J. Enzyme Inhib. Med. Chem.*, 2022, **37**, 135–144.
47 M. R. Akbarpour, F. Farajnezhad, A. H. Poureshagh, S. Moniri Javadhesari and H. S. Kim, Synthesis and Characterization of Copper-Doped Fluorohydroxyapatite Coatings for Biomedical Applications: Influence of Simultaneous Anodizing Treatment on AZ31 Alloy Substrate and Ultrasonic Agitation During Electrodeposition Process, *Met. Mater. Int.*, 2025, **31**, 2890–2900.
48 S. Liu, S. Li, X. E. Cao and S. Choi, An ultra-fast and eco-friendly recycling process for spent LIBs using deep eutectic solvents: mechanism and life-cycle insight, *Green Chem.*, 2025, **27**, 14648–14657.
49 X. Zhu, C. Chen, Q. Guo, M. Liu, Y. Zhang, Z. Sun and H. Song, Ultra-fast recovery of cathode materials from spent LiFePO4 lithium-ion batteries by novel electromagnetic separation technology, *Waste Manage.*, 2023, **166**, 70–77.
50 D. Song, J. Yu, M. Wang, Q. Tan, K. Liu and J. Li, Advancing recycling of spent lithium-ion batteries: From green chemistry to circular economy, *Energy Storage Mater.*, 2023, **61**, 102870.
51 X. Zhang, Q. Xue, L. Li, E. Fan, F. Wu and R. Chen, Sustainable Recycling and Regeneration of Cathode Scraps from Industrial Production of Lithium-Ion Batteries, *ACS Sustainable Chem. Eng.*, 2016, **4**, 7041–7049.
52 M. Wang, Q. Tan, L. Liu and J. Li, A Facile, Environmentally Friendly, and Low-Temperature Approach for Decomposition of Polyvinylidene Fluoride from the Cathode Electrode of Spent Lithium-ion Batteries, *ACS Sustainable Chem. Eng.*, 2019, **7**, 12799–12806.
53 S. C. Mun, Y. H. Jeon and J. H. Won, Progress and challenges for replacing n-methyl-2-pyrrolidone/polyvinylidene fluoride slurry formulations in lithium-ion battery cathodes, *Prog. Nat. Sci.*, 2024, **34**, 194–206.
54 K. K. Jena and D. S. Choi, Recycling of Cathode active materials from Spent Lithium-ion Batteries (LIBs): Effective Methodology for Environmental Remediation, *Mater. Chem. Phys.*, 2024, **311**, 128532.
55 Y. Fu, J. Schuster, M. Petranikova and B. Ebin, Innovative recycling of organic binders from electric vehicle lithium-ion batteries by supercritical carbon dioxide extraction, *Resour., Conserv. Recycl.*, 2021, **172**, 105666.

